Bioorganic Chemistry 86 (2019) 15–27

Contents lists available at ScienceDirect

Bioorganic Chemistry

journal homepage: www.elsevier.com/locate/bioorg

A combinatorial approach of structure-based virtual screening and molecular dynamics simulation towards the discovery of a highly selective inhibitor for VP9 coat protein of Banna virus

Parikshit Moitra

Technical Research Centre, Indian Association for the Cultivation of Science, 2A & 2B Raja SC Mullick Road, Jadavpur, Kolkata 700032, West Bengal, India

ARTICLE INFO

Keywords:
Banna virus
Viral envelope protein
Highly selective inhibitor
High-throughput virtual screening
Molecular dynamics simulation

ABSTRACT

Structure based virtual screening of two libraries containing 27,628 numbers of antiviral compounds was used to discover a few of the potent inhibitor molecules against Banna virus (BAV). Cross-docking studies with many common interfering proteins provided five of the highly selective inhibitor for BAV. Analyses of the leading molecules with ADME-Tox filtering tool and atomistic molecular dynamics simulation studies finally discovered a benzoxazolone derivative as one of the most promising molecules towards the highly selective inhibition of BAV. The theoretical calculations are also supported by the experimental evidences where the interactions between the hit ligand and a model peptide sequence, mimicking the VP9 protein of BAV, were studied. Overall the development of a personalized therapeutic towards the highly selective inhibition of BAV is discussed herein for the first time in literature.

1. Introduction

Banna virus (BAV) became one of the latest members of emerging infectious diseases across the world, declared by the Centre for Disease Control and Prevention (CDC) in the recent past [1]. The virus was isolated from mosquitoes, ticks, pigs, cattle and human encephalitis patients and found to be widely distributed throughout Southeast Asia. This demonstrated the BAV phylogeny as regionally variant [2,3]. The epidemiology of this particular virus remains poorly understood till date. It was reported that BAV is accountable for encephalitis in humans in conjuction with Japanese encephalitis virus (JEV), which is the most important encephalitis causing virus around the world. JEV reported to cause ~35–50 thousand cases annually with a mortality rate of almost 25–30% in Asia alone [4]. Hence it can be said that because of the similarity between BAV and JEV, the infection caused due to BAV may be underreported. Moreover, there is no specific treatment for this viral infection even today and hence the treatment solely lies on the reduction of severity of the symptoms by the hosts' immune system. Again the clinical features of BAV infection are non-specific and require the use of expensive laboratory techniques, like reverse transcription polymerase chain reaction (RT-PCR) assay [5] and enzyme-linked immunosorbent assay (ELISA) [6] for its diagnosis. In this regard, small molecule based biosensors are in high demand in the recent era of modern science [7–10] and following this, scientists are interested to develop a personalized therapeutic with high selectivity towards BAV.

BAV (genus Seadornavirus, family Reoviridae) [11] is an arbovirus, primarily transmitted by the mosquitoes of genus Culex [12]. This double-stranded, non-enveloped RNA virus is generally enclosed with an icosahedral protein coat, where VP4 and VP9 form the outer capsid layer [13,14]. The structure of VP9, outer coat protein of BAV, was determined by Jaafar et al. through X-ray crystallography [15]. Interestingly, it was also shown that the trimeric VP9 was involved in the cellular internalization process of the virus and hence VP9 played a determinant role in viral infectivity. Therefore if a molecule can be designed which specifically interacts and inhibits the action of the trimeric VP9 of BAV, it is possible to inhibit the progression of the infection caused by BAV.

With this goal in mind, a database of 27,628 numbers of antiviral compounds were undertaken for structure based high throughput virtual screening [16–20] with the virus coat protein of Banna virus, VP9 (PDB ID: 1W9Z). Both the virtual screening workflow and cross-docking studies with many common interfering proteins for BAV were carried out which led to the discovery of five molecules for the selective inhibition of BAV. Further analyses of these five molecules with ADME-Tox filtering tool and atomistic molecular dynamics simulation finally provided one of the most promising molecules for the highly selective inhibition of Banna virus. The theoretical calculations are also supported by the experimental evidences where interactions between the hit ligand and a model peptide sequence, mimicking the VP9 of BAV, were studied. Overall this study discusses the development of a

E-mail address: Parikshit.Moitra@iacs.res.in.

https://doi.org/10.1016/j.bioorg.2019.01.021
Received 5 October 2018; Received in revised form 6 January 2019; Accepted 9 January 2019
Available online 12 January 2019
0045-2068/

personalized therapuetic against BAV and thus offers opportunity for future development of a more potent inhibitor of Banna virus examining the structure-activity relationships of the most promising benzoxazolone derivative.

2. Results and discussion

2.1. Virtual Screening

A combination of Asinex [21] and Enamine [22] databases containing 13,322 numbers of antiviral compounds were screened against the capsid protein of Banna virus, VP9 (PDB ID: 1W9Z). At first, a phase database was prepared taking all these molecules through the Phase database preparation module of the Schrodinger molecular modeling suite [23]. A maximum of 50 different conformers were generated, minimized and different ionization states were created from these molecules at pH 7.0 ± 2.0 using Epik module of Schrodinger molecular modeling suite. The high energy ionization/tautomer states and ligands with reactive functional groups were removed. Thus a library of 27,628 numbers of antiviral molecules was generated for the screening studies with VP9 protein of Banna virus. This database was then used for *in silico* receptor based virtual screening workflow using the Glide (Grid-based ligand docking with energetics) module [24] of the Schrodinger molecular modeling suite (Fig. 1).

Now the recombinant VP9 has a trimeric structure as revealed by X-ray crystallography [15] and hence the protein sequence was divided into three separate chains as processed by the Protein preparation wizard [25] of Schrodinger molecular modeling suite (Fig. S1). These chains were analyzed by SiteMap module of the Schrodinger molecular modeling suite [26,27] to identify their binding site and assessing druggability. It was seen that chain A and B had four different binding sites, whereas the chain C had five separate binding sites (Figs. 2, S2 and S3). But the site 1 and 2 of chain A had the highest sitescore value (Fig. 2) representing themselves as the most preferable druggable sites in the whole protein sequence of VP9 of BAV. Although the site 1 and 2 of chain A were the hypothetical binding sites for VP9 of BAV, but in absence of any literature, demonstrating the experimental binding sites for this viral protein, these sites could be considered as the most preferable druggable sites for further docking studies.

Now the Glide virtual screening workflow (VSW) consists three steps of docking of increasing precisions, i.e. high-throughput virtual screening (HTVS), standard precision (SP) and extra-precision (XP) [28–30]. All the 27,628 numbers of molecules were initially screened by HTVS mode and the top 10% molecules from the output were undertaken for docking in SP mode. Top 5% molecules from the SP docking output were further screened by XP mode and the final output was filtered for a docking score of ≤ -7.00 [31,32] and druglikeness according to the Lipinski's rule of five [33]. Only twelve and seventeen numbers of ligands, for the site 1 and site 2 of chain A of VP9 respectively, were selected from the VSW process. These ligands were represented in Tables 1 and 2 for site 1 and site 2 of chain A of VP9 respectively along with their structures and docking scores.

Again the Pubchem database for antiviral compounds was considered for the screening studies and fifteen different compounds were undertaken for docking studies with the site 1 and site 2 of chain A of VP9 protein. It was observed that none of these fifteen ligands crossed the docking score threshold of ≤ -7.00 (Table S1) and hence these were not considered for further screening studies.

2.2. Determining the selectivity of the ligands towards Banna virus

Now it is necessary to identify those ligands among these twenty nine ligands which are highly selective for VP9 of Banna virus. Therefore these twenty nine ligands were undertaken for cross-docking studies. The common viral proteins which can interfere in the selective inhibition of BAV are bluetongue virus, dengue virus, encephalitis virus, rotavirus and cypovirus. A pool of these interfering protein sequences were then extracted from RCSB Protein Data Bank and their interactions with the twenty nine ligands were monitored. The particular protein-ligand interaction was considered to be interfering for the selective inhibition of VP9 of BAV, only when the docking score of the protein-ligand complex became ≤ -7.00 [31,32]. It was found that some of the ligands interacted strongly with the VP7 protein of bluetongue virus (1BVP), dengue 2 virus envelope protein (1OKE), conserved core domain of venezualan equine encephalitis capsid protein (1EP5 and 1EP6), rotavirus strain DS-1 VP8* core (2AEN), japanese

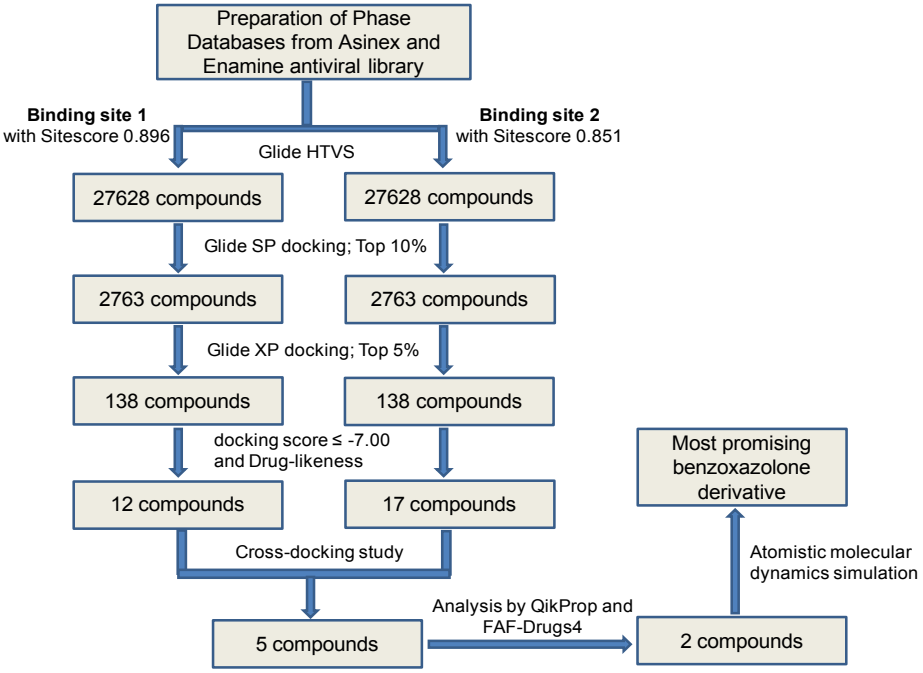

Fig. 1. Workflow demonstrating the combinatorial approach of docking based virtual screening and molecular dynamics simulation for the identification of most promising inhibitor molecule for Banna virus.

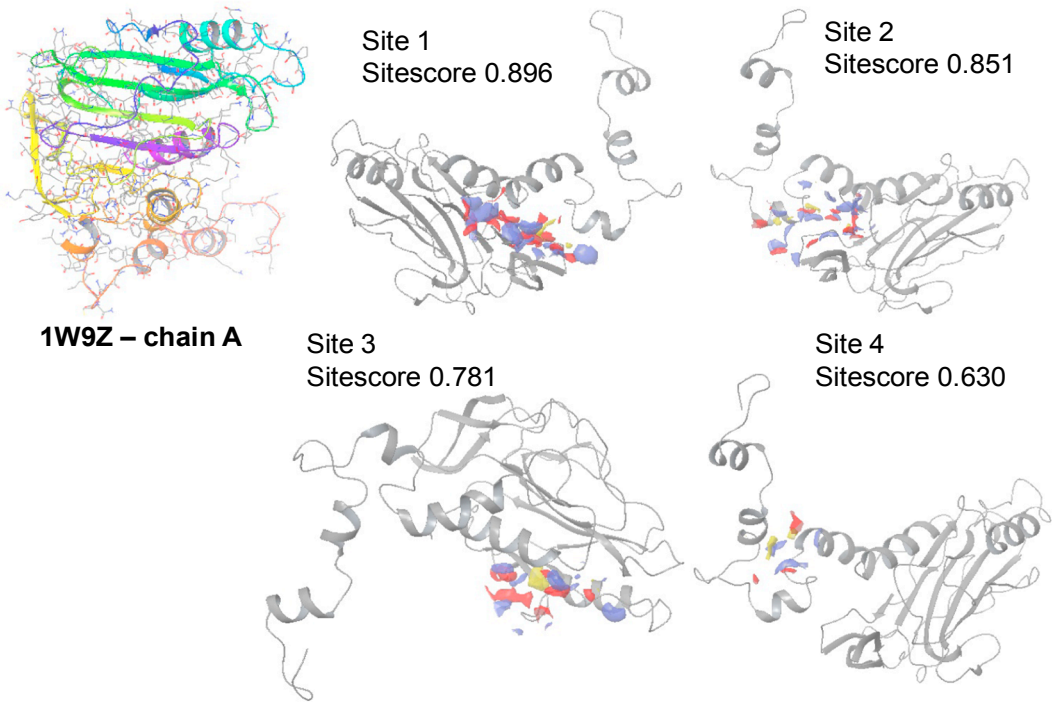

Fig. 2. Representation of the binding sites in chain A of 1W9Z protein sequence as predicted by SiteMap module of the Schrodinger molecular modeling suite. Here H-bond acceptor, H-bond donor, hydrophobic and surface are presented by red, blue, yellow and grey color respectively.

encephalitis virus envelope protein (3P54), transcribing cypovirus (3J17), full-length japanese encephalitis virus NS5 (4K6M), apo porcine rotavirus TFR-41 VP8* (5CA6), P[19] rotavirus VP8* (5VKI) and japanese encephalitis virus (5WSN). It was also observed that none of these twenty nine ligands interacted well with the protein sequences of dengue virus (1K4R), rhesus rotavirus VP4 (1KRI), dengue 2 virus envelope protein (1OAN), envelope protein of tick-borne encephalitis virus (1URZ), rhesus rotavirus VP5 antigen domain dimer (2B4H), rhesus rotavirus VP8* (2P3I), porcine CRW-8 rotavirus VP8* (3SIS), cell attachment protein VP8* of a human rotavirus (4DRR) and human rotavirus K8 VP8* (5CB7). The details of the protein-ligand interactions have been tabulated in Table 3 and it can be concluded that five of the ligands among the twenty nine ligands are highly selective for VP9 of Banna virus.

The chemical structures of these five ligands together with their binding and interaction sites with the chain A of VP9 of Banna virus is represented in Fig. 3. All of the protein-ligand binding and interaction sites were visualized by Maestro module of the Schrodinger modeling suite [34]. This is observed that primarily H-bonding interaction is responsible for the stabilization of the protein-ligand complexes. Moreover, a salt-bridge type of interaction can be seen between the ammonium group of the ligand (code: Lig-553) and ASP-193 of the protein (Fig. 3b) and pi-cation type stabilizing interaction can be visualized between the phenyl ring of the ligand (code: Lig-2369) and ARG-98 of the protein (Fig. 3a). Because of the high selectivity of these five ligands towards the outer coat protein, VP9, of BAV, it can be said that these ligands can also be used for the selective diagnosis of BAV.

Further the physico-chemical properties were now calculated by the QikProp module of Schrodinger molecular modeling suite. A few of these properties were compared in Table 4. It is to be noted that dipole, SASA, FOSA, CIQPlogS, donorHB, acceptHB, IP and EA indicate dipole moment of the molecule, total solvent accessible surface area in square angstroms, hydrophobic component of the SASA, conformation-independent predicted aqueous solubility of the solute, estimated number of hydrogen bonds that would be donated by the solute to water molecules, expected number of hydrogen bonds that would be accepted by the solute from water molecules, PM3 calculated ionization potential and PM3 calculated electron affinity respectively. The values of donorHB and acceptHB may be non-integer as they are calculated as an average of a number of configurations of a ligand. %Human oral absorption is based on a quantitative multiple linear regression model and uses a knowledge-based set of rules including number of rotatable bonds, logP, solubility and cell permeability of a ligand. It may be particularly emphasized that the values of donorHB and acceptHB for lig-2369 are relatively lower than others, which may be a reason for this ligand to preferentially interact with the receptor protein, VP9 of Banna virus. Also the predicted value of %human oral absorption is much higher for lig-2369 than others. These properties may provide an advantage for lig-2369 over others as a plausible potent inhibitor for the VP9 coat protein of Banna virus.

2.3. Analyzing the ADMET properties of the lead ligands

Now it is necessary to determine the ADMET properties and binding efficiency of these ligands to identify a particular ligand as the most efficient one for the selective inhibition of BAV. The lead five ligands were then processed with FAFDrugs4 (Free ADME-Tox Filtering Tool) [35], which is an advanced program to perform computational prediction on some properties like adsorption, distribution, metabolism, excretion and toxicity to support hit selection before investing efforts on ligand synthesis or ordering. It was interesting to note that none of these five ligands are PAINS moieties, i.e. Pan Assay Interference Compounds, those appear as common hitters in many high throughput screening processes [36]. But lig-553, lig-1484 and lig-2678 were rejected by the program as they are not protein-protein interaction inhibitors [37,38]. Moreover, lig-1484 and lig-2678 violated the golden triangle rule [39] and hence likely to have problem in clearance, metabolic stability and oral absorption. Only the lig-2369 and lig-1762 were accepted by the program as the potent hits. Both of these ligands passed the computational criteria for oral bioavailability, i.e. Lipinski rule of five, Veber rule, Egan rule and Bayer oral physchem score. These two ligands also cleared the relevant criteria for drug safety profiling, i.e. GSK 4/400 rule, Pfizer 3/75 rule, phospholipidosis non inducer and Lilly medchem rules.

Table 1
Output from the virtual screening workflow with the site 1 of chain A of VP9 protein, Banna virus.

Serial no.	Ligand code	Structure	Docking score
1	Lig-3257	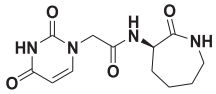	−9.22
2	Lig-2068	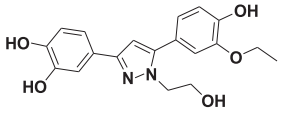	−8.65
3	Lig-1130	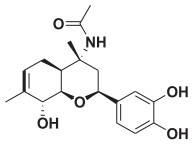	−8.00
4	Lig-2369	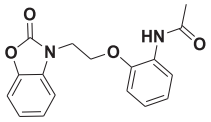	−7.83
5	Lig-2062	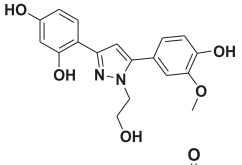	−7.71
6	Lig-1452	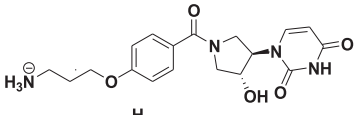	−7.38
7	Lig-3080	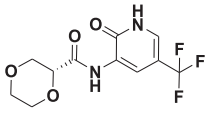	−7.37
8	Lig-3152	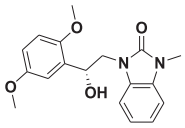	−7.36
9	Lig-1259	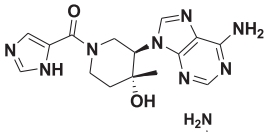	−7.32
10	Lig-1151	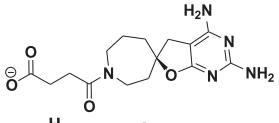	−7.32
11	Lig-2678	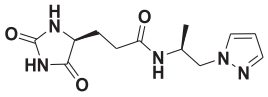	−7.29
12	Lig-2063	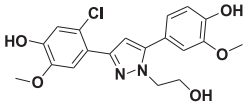	−7.00

2.4. Analysis by molecular dynamics simulation

Although FAFDrugs4 indicated about the efficient druggability of the two ligands only, i.e. lig-2369 and lig-1762, it may be good idea to evaluate the stability of the protein-ligand complexes for all the five lead ligands with atomistic molecular dynamics simulation. In this regard, GROMACS 4.6.5 [40–42] software was chosen to set up a simulation system containing the protein, VP9, in complex with a particular ligand as obtained from the XP docking mode. Each of the complexes were solvated in a similar volume of tip4p water box, energy minimized, equilibrated in NVT and NPT ensemble respectively and finally undertaken for a 20 ns of production run in NPT ensemble at 300 K [43–44]. It was observed that the average coulomb (short range) energy for the complexes with lig-1484 and lig-2369 is higher than others (Fig. 4a), whereas the Lennard-Jones potential for the complex with lig-2369 is the highest among all (Fig. 4b). This clearly indicated the better binding ability of lig-2369 with the VP9 protein of BAV leading to higher stability of the complex than any others. The primary interaction sites for the lig-2369 have been represented in Fig. 4d, as obtained from the simulation of 20 ns, which further confirmed the

Table 2
Output from the virtual screening workflow with the site 2 of chain A of VP9 protein, Banna virus.

Serial no.	Ligand code	Structure	Docking score
1	Lig-2058	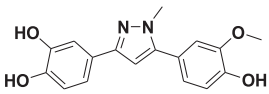	−8.40
2	Lig-2057	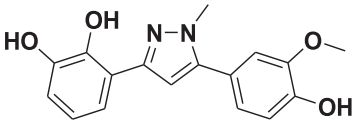	−7.87
3	Lig-431	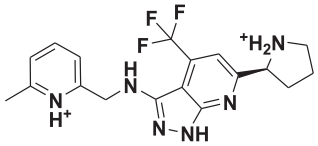	−7.78
4	Lig-2060	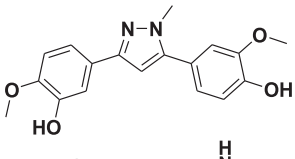	−7.62
5	Lig-662	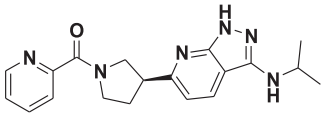	−7.52
6	Lig-2719	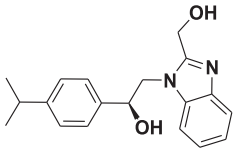	−7.45
7	Lig-2056	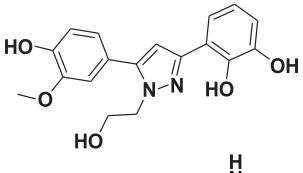	−7.44
8	Lig-360	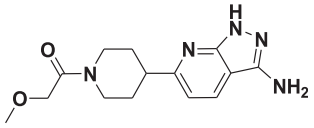	−7.44
9	Lig-1484	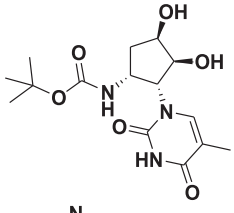	−7.34
10	Lig-553	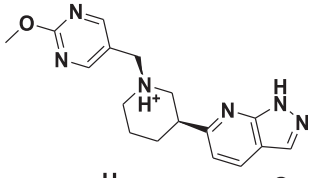	−7.19
11	Lig-663	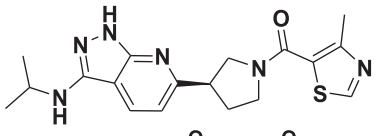	−7.14
12	Lig-1755	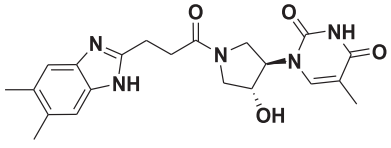	−7.13

(*continued on next page*)

Table 2 (*continued*)

Serial no.	Ligand code	Structure	Docking score
13	Lig-185a	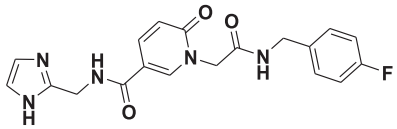	−7.09
14	Lig-3183	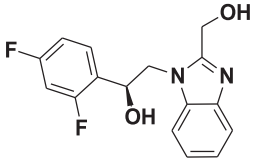	−7.06
15	Lig-185b	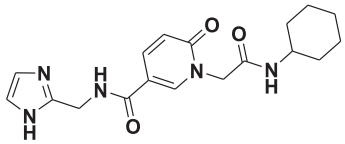	−7.04
16	Lig-1656	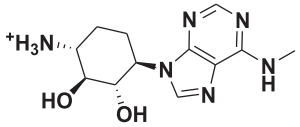	−7.03
17	Lig-1762	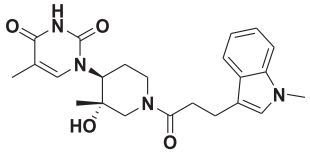	−7.00

Table 3
Results from the cross-docking studies showing the selectivity of the ligands towards Banna virus.

Ligand code	Interfering proteins with docking score
Lig-3257	5CA6 (−7.6); 5VKI (−7.301); 5WSN (−7.022)
Lig-2068	1EP6 (−7.050); 1OKE (−7.104); 2AEN (−7.332); 5CA6 (−7.717)
Lig-1130	2AEN (−7.557); 5WSN (−7.998)
Lig-2369	No preferential binding with these protein series having docking score of ≤ −7.00
Lig-2062	1EP5 (−7.787); 1OKE (−7.349); 2AEN (−7.276); 5WSN (−7.203)
Lig-1452	1BVP (−7.580); 2AEN (−7.223); 5VKI (−7.647)
Lig-3080	5CA6 (−7.787); 5WSN (−7.192)
Lig-3152	5WSN (−8.427)
Lig-1259	5CA6 (−7.671); 5WSN (−7.827)
Lig-1151	4K6M (−7.247); 5WSN (−8.391)
Lig-2678	No preferential binding with these protein series having docking score of ≤ −7.00
Lig-2063	1EP5 (−7.144); 5WSN (−7.294)
Lig-2058	1EP5 (−7.344); 2AEN (−7.208); 5CA6 (−8.172)
Lig-2057	1EP5 (−7.664); 1EP6 (−7.237); 5CA6 (−8.165); 5VKI (−8.504)
Lig-431	1BVP (−7.836); 5VKI (−7.721)
Lig-2060	5CA6 (−8.155)
Lig-662	5CA6 (−8.839); 5CA6 (−7.626); 5VKI (−7.416); 5WSN (−7.046)
Lig-2719	5CA6 (−8.260); 5WSN (−8.292)
Lig-2056	1EP5 (−7.868); 1EP6 (−7.100); 1OKE (−7.193); 2AEN (−7.518); 5CA6 (−7.099); 5VKI (−7.969); 5WSN (−7.746)
Lig-360	5WSN (−7.099)
Lig-1484	No preferential binding with these protein series having docking score of ≤ −7.00
Lig-553	No preferential binding with these protein series having docking score of ≤ −7.00
Lig-663	1OKE (−7.381); 5CA6 (−7.975); 5VKI (−8.256); 5WSN (−7.108)
Lig-1755	1EP6 (−7.778); 3P54 (−7.631); 5CA6 (−7.681); 5WSN (−8.013)
Lig-185a	1OKE (−7.468); 5CA6 (−8.756); 5WSN (−8.892)
Lig-3183	5CA6 (−7.767); 5WSN (−7.848)
Lig-185b	1OKE (−7.058); 2AEN (−7.018); 5CA6 (−7.527); 5WSN (−7.024)
Lig-1656	3J17 (−7.335); 5WSN (−7.092)
Lig-1762	No preferential binding with these protein series having docking score of ≤ −7.00

docking results. The root mean square deviation plot for the complex stabilized with lig-2369 over the simulation timescale is shown in Fig. S4. It was also ascertained that the average number of hydrogen bonds for the protein-ligand complexes with lig-1484 and lig-2369 was higher than other complex series studied herein (Fig. 4c).

2.5. Evaluation of the stability of the conformal states and binding site interactions of chain A of VP9 of Banna virus

In order to validate the stability of the conformal states from which the ligands for preferential binding site were derived, the chain A of VP9 protein of Banna virus (PDB ID: 1W9Z) was simulated for 20 ns.

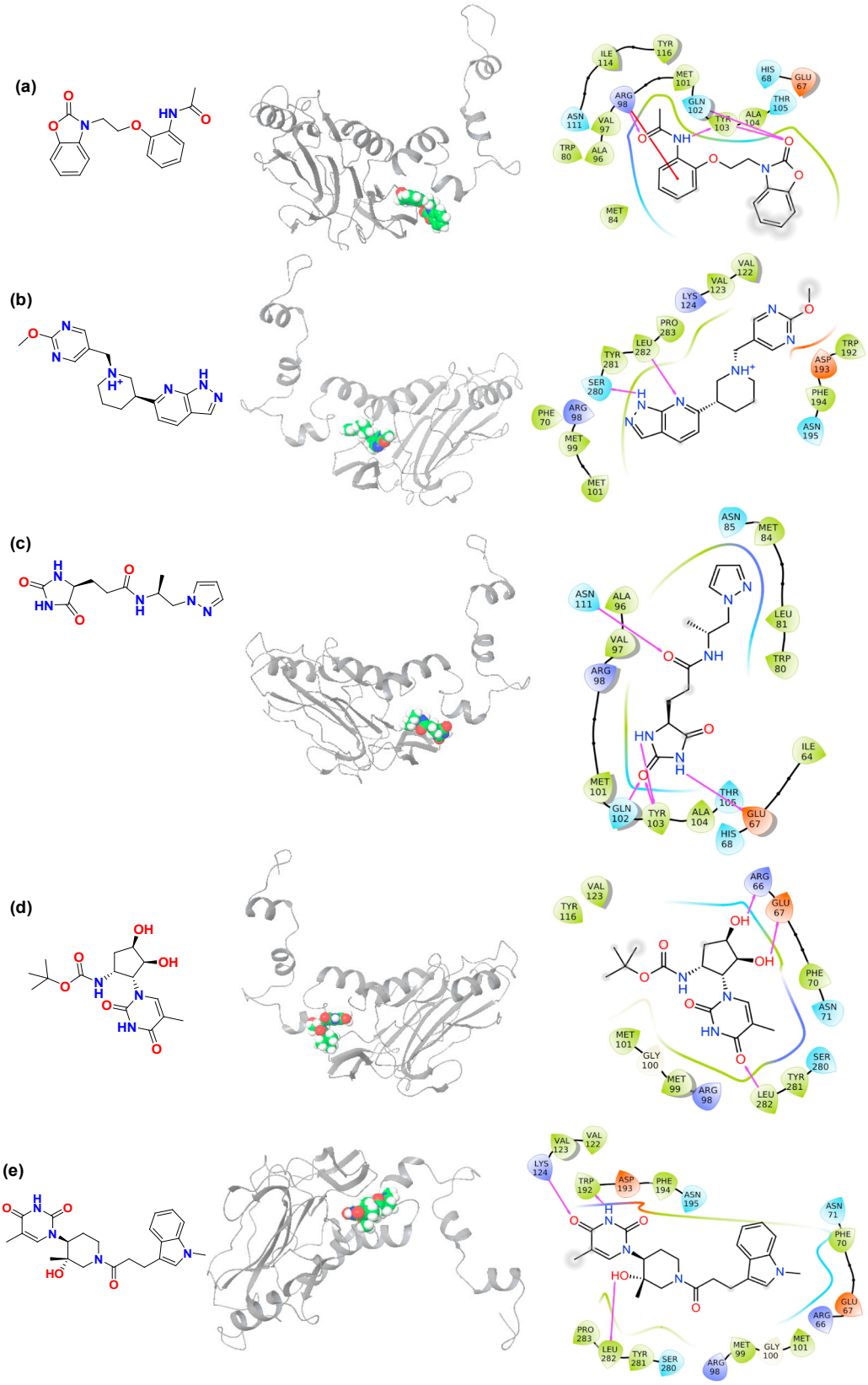

Fig. 3. The chemical structures along with their binding and interaction sites with the chain A of VP9 of Banna virus is represented herein for the lead five ligands: (a) Lig-2369, (b) Lig-553, (c) Lig-2678, (d) Lig-1484 and (e) Lig-1762. The binding site of the ligands with the protein is shown next to the chemical structures of the ligands, where the protein is represented by its secondary structure and the ligand is presented by space filling model. The interactions sites of the ligands with the protein are shown to the right of the binding site representation. Here the negatively charged amino acids, positively charges amino acids, glycine, hydrophobic and polar residues are represented with orange, blue, yellow, green and indigo color codes respectively. The H-bonding and pi-cation interactions are highlighted with pink and red colored arrows respectively.

The trajectory was analyzed and it was found that there were only four clusters over the simulation runtime. The structures were collected after each 20 ps of simulation runtime and thus 1001 numbers of frames were considered for clustering. It was observed that one of the conformal states appeared 805 times (~80%) among the total frames appeared during the simulation (Fig. S5). The middle structure of this particular cluster was taken into consideration for the prediction of its binding sites through SiteMap module of Schrodinger molecular modeling suite [26,27]. The sitescore and residues of the binding pockets were found to be comparable for both the protein sequences before and

Table 4
Comparison of some of the physico-chemical properties of the five lead ligands as predicted by QikProp module.

Ligand code	Dipole	SASA	FOSA	CIQPlogS	donorHB	acceptHB	IP (eV)	EA (eV)	%Human oral absorption
Lig-2369	4.205	516.340	123.945	−3.991	1.0	6.25	8.762	0.514	91.101
Lig-2678	7.434	548.352	211.010	−1.942	3.0	7.5	9.801	−0.039	59.339
Lig-553	7.228	574.322	345.843	−2.825	4.0	9.4	9.414	0.576	62.267
Lig-1484	2.728	611.340	276.446	−3.313	1.5	6.5	9.238	0.745	82.087
Lig-1762	5.589	735.939	352.355	−5.200	2.0	7.25	8.310	0.412	79.688

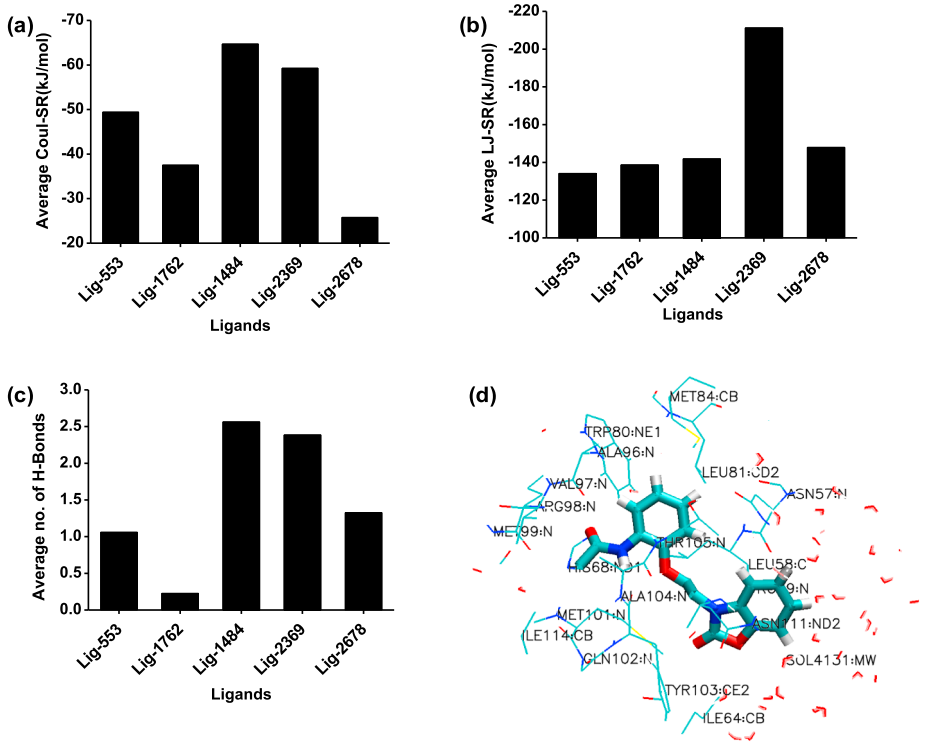

Fig. 4. Plots for average (a) Coulomb and (b) Lennard-Jones potential for the protein-ligand complexes are represented. The average numbers of hydrogen bonds present in the complexes are shown in (c) and the primary interaction sites for the lig-2369 are represented in (d) over the simulation timescale.

Table 5
Comparison of the sitescore and residues of the major binding sites among the protein sequences.

Chain A of VP9 of Banna virus	Site	Sitescore	Number of residues
Before simulation as obtained from RCSB database	Site 1	0.896	67,68,80,81,84,85,86,88,90,91,92,93,94,95,96,97,98,101,102,103,104,105,109,111,114,265
	Site 2	0.851	63,66,67,70,71,98,99,100,101,102,122,123,124,192,193,194,195,280,281,282
After simulation of 20 ns	Site 1	0.873	63,64,65,66,67,68,77,80,81,84,85,86,92,93,94,95,96,98,101,102,103,104,105,109,111,114
	Site 2	0.824	67,70,71,98,99,100,101,124,189,190,192,193,194,195,280,281,282,283
Simulated protein-ligand complex with lig-2369	**Site 3**	1.016	56,57,58,59,64,65,68,80,81,84,85,93,94,96,97,98,99,100,101,103,104,105,109,110,111,114,116
	Site 4	0.675	40,41,42,43,44,45,48,49,52,53,69,70,72,73,74,76,77
Simulated protein-ligand complex with lig-2678	**Site 5**	0.924	67,68,70,80,84,85,86,91,92,93,94,95,96,97,98,101,103,104,105,106,107,109,114,261,262,276
	Site 6	0.722	147,150,151,152,153,154,155,180,182,241,242,244,246,247,248,249,250,251,252,253,256
Simulated protein-ligand complex with lig-1762	**Site 7**	0.997	63,66,67,70,71,98,99,100,101,193,194,195,197,198,274,277,278,279,280,281,282,283
	Site 8	0.803	145,147,151,152,153,154,156,158,163,164,165,182,184,185,186,236,237,239,241
Simulated protein-ligand complex with lig-1484	**Site 9**	0.862	63,66,67,68,70,71,77,98,99,101,111,124,192,193,194,280,281,282,283
	Site 10	0.584	150,151,152,155,156,157,249,253,256

after MD simulation (Table 5). Therefore it may be concluded that the conformal states for chain A of VP9 protein of Banna virus were quite dominant in nature.

Further to confirm the binding site stability of the protein sequences, isolated from the respective protein-ligand complexes after their MD simulation of 20 ns, SiteMap calculations were carried out. It was previously noted that lig-2369 and lig-2678 interacted preferentially with site 1 of chain A, whereas the other three ligands among the five lead ligands showed their preferential binding with the site 2 of chain A (Tables 1 and 2). The lig-1762 was screened according to the ADMET profile of the ligands and lig-1484 was preferred according to the H-bond and coulomb energy (short range) profile of the ligands (Fig. 4) together with the lig-2369 in all the cases. For all of these protein-ligand complexes, the middle structure of the most prevailing cluster was chosen for the SiteMap calculations. The detailed sitescore and residues of the two binding pockets were tabulated in Table 5 for each of the cases. It was observed that the proteins derived from the corresponding complexes having lig-2369 (site 3) and lig-2678 (site 5) bind preferentially with the comparable site 1 of the original protein sequence, whereas the proteins derived from the complexes having lig-

1762 (site 7) and lig-1484 (site 9) had their preference for the analogous site 2 of the protein. The other binding sites (site 4, 6, 8 and 10) for the protein-ligand complexes were neglected due to their low sitescore value.

2.6. Experimental evidences

The ligand, N-[2-[2-(2-oxo-3(2H)-benzoxazolyl)ethoxy]phenyl]-acetamide (lig-2369), was thus found to be the most promising ligand, among all the 27,628 numbers of antiviral compounds studied herein, for the highly selective inhibition of the infection caused by Banna virus. The compounds, derived on the benzoxazolone heterocycle, received considerable amount of attention among the medicinal scientists because of their ability to mimic metabolically stable templates like phenol or catechol. The heterocycle and pyrocatechol have similar physico-chemical properties like pKa's, chemical reactivity and electronic charge distribution, etc. [45]. Pharmacological applications of this benzoxazolone heterocyclic template include antibacterial, antifungal, analgesic, anticonvulsant, anti-inflammatory, anticancer and anti-HIV, etc. [46–49]. Therefore the benzoxazolone template was declared as the "privileged scaffold" in medicinal chemistry due to its enormous therapeutic importance.

It can be said from the results of the high-throughput virtual screening, cross-docking and molecular dynamic simulation that the high selectivity and preferential binding ability of the lig-2369 towards the capsid protein, VP9, of Banna virus will be primarily responsible for the viral infectivity [15]. Interestingly it was observed from both the docking and simulation studies that the active site residue of VP9, which interacted strongly with the lig-2369, was in a continuous stretch unlike the other ligands and hence could be mimicked easily. It was thought that in absence of real samples of BAV, the demonstration of direct target binding of the chosen ligand could be shown with a model peptide sequence which could mimic the active site residue of VP9. Accordingly a model peptide sequence, Ala-Val-Arg-Met-Gly-Met-Gln-Tyr-Ala (AVRMGMQYA), was synthesized, purified by reverse phase high performance liquid chromatography (Fig. S6) and characterized using mass spectroscopy, MALDI-MS (Fig. S7). The details of the solid phase synthesis, purification and characterization protocols were provided in the supporting information. The ligand, N-[2-[2-(2-oxo-3(2H)-benzoxazolyl)ethoxy]phenyl]-acetamide (lig-2369), was procured from a local supplier and characterized for its purity by different analytical techniques like ^{1}H NMR, ^{13}C NMR, mass spectroscopy (ESI-MS) and its HPLC profile (Figs. S8–S11).

Now to ascertain the binding efficiency of the hit ligand with the model peptide sequence, UV–Visible titration was performed with the increasing concentration of the ligand, added to a solution of the model peptide in 1X PBS buffer (pH 7.4). It was observed that the dissociation constant of the complex, formed with lig-2369, was ~68.6 μM (Fig. 5a), whereas the dissociation constant of the complex, formed with lig-2678, was found to be > 200 μM. Although the data represented a weak apparent compound activity, it can further be postulated that the effective inhibitory concentration of the benzoxazolone derivative (lig-2369) for BAV might be in the sub-micromolar range when tested against the real samples of BAV. The relatively low value of dissociation constant for the lig-2369 indicated the plausible formation of a fairly stable complex of the ligand with the capsid protein, VP9, of Banna virus. Now it is known that the infection caused by BAV has a close similarity with the Japanese encephalitis virus (JEV) [3] and hence the selectivity and better binding ability of the benzoxazolone derivative with the VP9 of Banna virus was further confirmed by determining the dissociation constant of the complex formed with nitazoxanide and the model peptide sequence. The nitazoxanide is a well-known broad-spectrum antiviral drug, widely used for the treatment of patients suffering from encephalitis [4]. This was found that the concentration of nitazoxanide (146.8 μM), needed to form a stable complex with the model peptide (AVRMGMQYA), was much higher than was observed in case of the benzoxazolone derivative (lig-2369) (Fig. 5b). Thus it can be said that the specific and relatively strong affinity of the benzoxazolone derivative (lig-2369) towards the model peptide sequence of VP9 of Banna virus will ultimately lead to the selective inhibition of the infection caused by BAV.

Further the existence of the peptide-ligand complex at 1:1 stoichiometry between the model peptide and the benzoxazolone derivative (lig-2369) in a buffered solution (1X PBS buffer of pH 7.4) was determined by acquiring the mass spectra of the solution in linear positive ion mode in the *m/z* range of 700–2000 Da using an Ultraflextreme MALDI-TOF/TOF mass spectrometer. The mass spectra showed the presence of *m/z* peak at 1376.594 Da ($M_{peptide} + M_{ligand} + K^{+}$) which represents the formation of a stable 1:1 complex between the ligand and peptide (Fig. 6a). Further the complex was analyzed under the "LIFT" technique of MALDI LIFT-TOF/TOF mass spectrometry [50,51]. But before analyzing the fragmented masses for the complex, it is important to understand the fragmented masses those can arise from the peptide itself. Therefore the peptide fragmentation had been studied and all the possible masses were shown in Fig. S12. Now the fragmented mass spectrum of the complex could be analyzed and the presence of multiple peaks indicating the formation of a stable 1:1 complex were monitored (Fig. 6b). Especially the *m/z* peaks at 1268.249, 1168.638, 1152.890, 958.085 and 942.110 could be assigned for $M(y8)_{peptide} + M_{ligand} + H$, $M(y7)_{peptide} + M_{ligand}$, $M(y7)_{peptide} - NH_3 + M_{ligand} + H$, $M(b6)_{peptide} + M_{ligand} - H$ and $M(b6)_{peptide} + M_{ligand} - NH_3$ respecively.

2.7. Comparing the model peptide sequence, AVRMGMQYA, with the VP9 of Banna virus

In order to probe the conformer dynamics of the model peptide, AVRMGMQYA, with the VP9 protein of Banna virus, initially the peptide sequence was energy minimized by B3LYP/6-31G* method in PCM solvent model using water in Gaussian 09 software. This energy minimized system was then used to build a simulation system using GROMACS 4.6.5 [40–42] software. The system was solvated in a tip4p water box, energy minimized, equilibrated in NVT and NPT ensemble

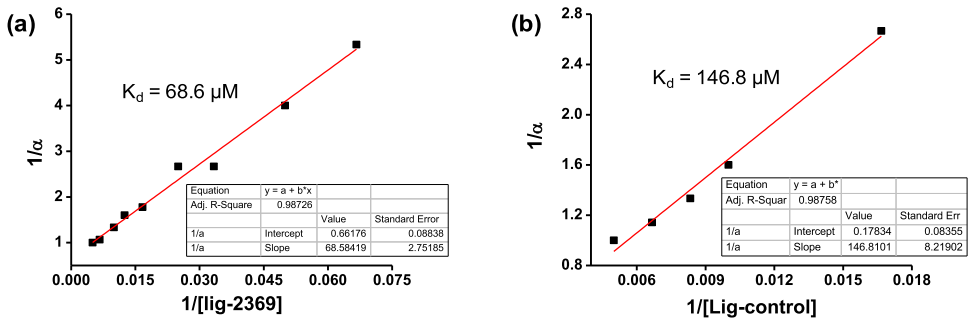

Fig. 5. Determination of dissociation constant of the complex, formed with the model peptide and (a) lig-2369; (b) control ligand (nitazoxanide), from UV–Visible titration.

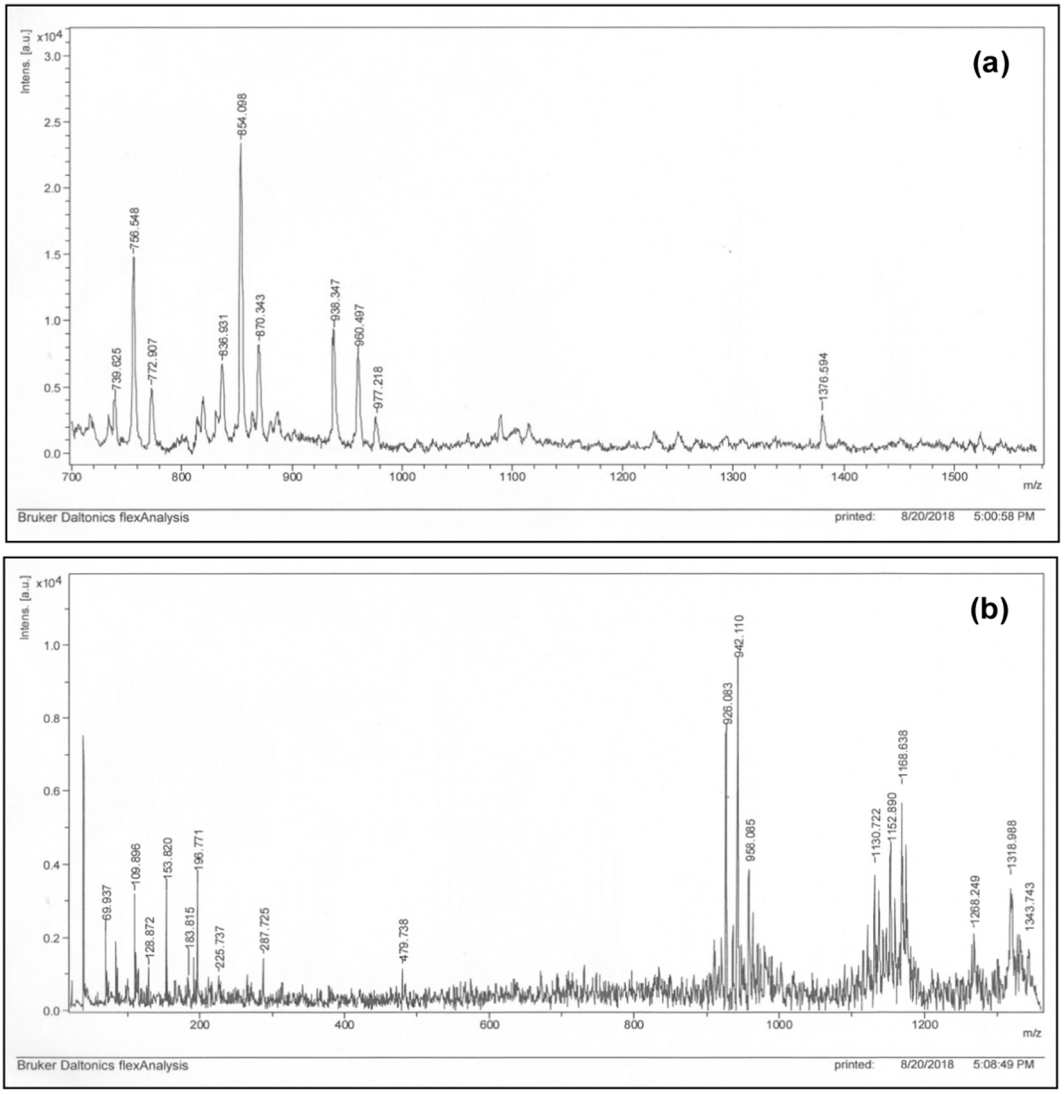

Fig. 6. (a) MALDI-TOF and (b) MALDI LIFT-TOF/TOF mass spectra of the peptide-ligand(2369) complex at 1:1 stoichiometry.

respectively and finally undertaken for 20 ns of production run (time-step 2 fs) in NPT ensemble at 300 K. OPLS-AA/L all-atom force field was used during the simulation. Root mean square deviation (RMSD) plot for the model peptide sequence, AVRMGMQYA, over the simulation timescale was shown in Fig. S13. The trajectory was analyzed in a similar manner and it was found that there were only three clusters over the simulation runtime. It was observed that one of the conformal states appeared 985 times (~98%) among the total 1001 frames appeared during the simulation. The middle structure of this particular cluster was taken into consideration, energy minimized in gaussian software and superimposed with the peptide sequence taken from the VP9 protein of Banna virus (Fig. 7c). It was found the RMSD for the poses was only 2.6369, which indicated reasonably similar conformal dynamics of the model peptide sequence with the VP9 of Banna virus. It was also observed that the model peptide sequence mostly remained as a random coil in the protein (Fig. 7a) which was comparable with the simulated dynamics of the peptide (Fig. 7b). The Ramachandran plot of the model peptide, generated over the simulation timescale, also supported the claim of random coil like conformer dynamics for the peptide (Fig. 7d).

Further to validate the binding site affinity of the model peptide as compared to the VP9 of Banna virus, Glide based docking was performed in SP mode. It was previously observed that lig-2369 and lig-2678 interacted strongly with site 1 of chain A, whereas lig-553, lig-1484 and lig-1762 interacted well with site 2 of chain A of VP9, Banna virus (Tables 1 and 2). It was further monitored that the model peptide sequence, AVRMGMQYA, had its strong binding affinity only for lig-2369 and lig-2678 than other three ligands (Fig. 3). Hence the binding affinity of the model peptide was evaluated for these two ligands, i.e. lig-2369 and lig-2678, which were also screened for study finally. It was observed that these two ligands had quite similar interaction sites with the model peptide sequence as it was found with the VP9 protein of Banna virus. It was also monitored that H-bonding interaction was primarily responsible for the stabilization of the peptide-ligand complexes (Fig. 8).

The docked model of the peptide-ligand complexes were then considered for simulation in a similar fashion. The complexes were solvated in a tip4p water box, energy minimized, equilibrated in NVT and NPT ensemble respectively and finally undertaken for a 20 ns of production run in NPT ensemble at 300 K. It was observed that the average coulomb (short range) energy for the protein-ligand complex with lig-2678 is more, whereas the Lennard-Jones (short range) potential for the complex with lig-2369 is higher (Fig. S14a). This clearly indicated the better binding ability of lig-2369 even with the model peptide sequence leading to higher stability of the complex than the other one. It was also seen that the average number of hydrogen bonds for the peptide-ligand complexes were almost similar for both the cases (Fig. S14b).

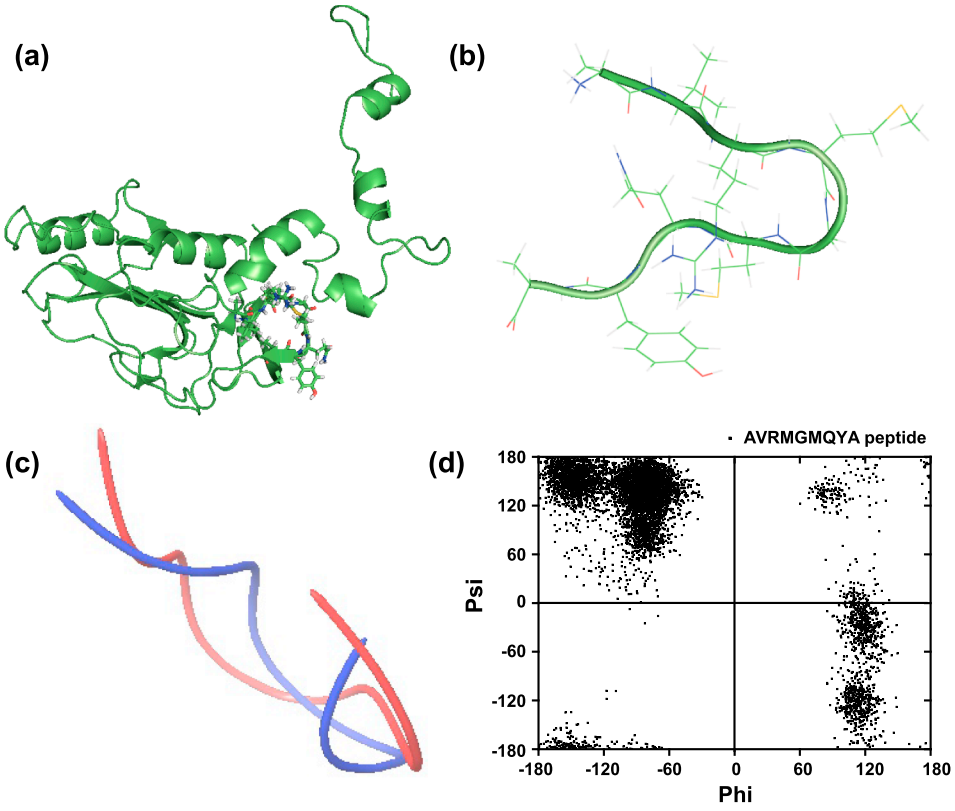

Fig. 7. Comparison of the secondary structure of the model peptide sequence, AVRMGMQYA, (a) inside the protein and (b) output from the 20 ns simulation run. The peptide structures as obtained from the protein (red in color) and from the simulation (blue in color) are superimposed in (c) and Ramachandran plot of the peptide generated over the simulation timescale is shown in (d).

3. Conclusions

A database of 27,628 numbers of antiviral compounds were undertaken for structure based high throughput virtual screening against the virus coat protein of Banna virus, VP9 (PDB ID: 1W9Z). The virtual screening workflow indicated 29 ligands as the promising ones. These ligands were further considered for cross-docking studies with many common interfering proteins. The leading five ligands were analyzed with ADME-Tox filtering tool and atomistic molecular dynamics simulation which finally indicated a benzoxazolone derivative as one of the

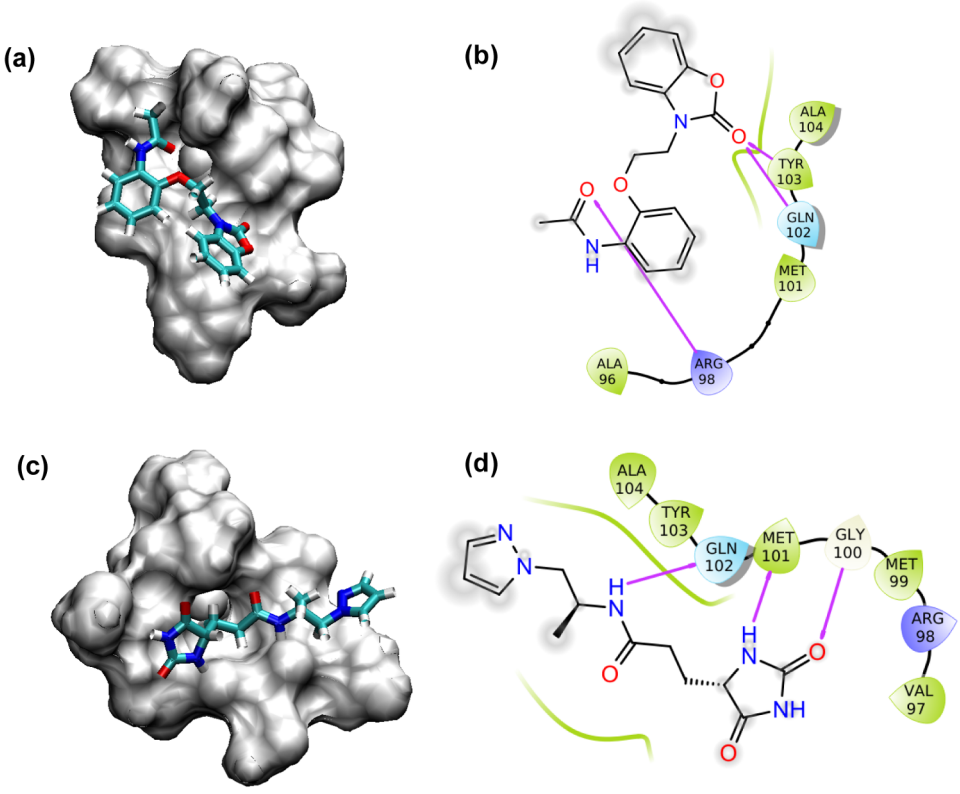

Fig. 8. The binding and interaction sites with the model peptide sequence, AVRMGMQYA, are represented herein for the final two ligands: (a) Lig-2369 and (b) Lig-2678. (a and c) The binding site of the ligands with the peptide is shown, where the peptide is represented by surface and the ligand is presented by ball and stick model. (b and d) The interactions sites of the ligands with the peptide are shown to the right of their binding site representation. Here the positively charged amino acids, glycine, hydrophobic and polar residues are represented with blue, white, green and indigo color codes respectively. The H-bonding interactions are shown with pink colored arrows.

most promising molecules towards the selective inhibition of Banna virus. The theoretical calculations are also substantiated by the experimental observations between the ligand and a model peptide sequence mimicking the VP9 of BAV. Thus it was established that the ligand, N-[2-[2-(2-oxo-3(2H)-benzoxazolyl)ethoxy]phenyl]-acetamide (lig-2369) could be used for the highly selective inhibition of Banna virus. It is noteworthy to mention that this kind of study for developing a personalized therapy towards the selective inhibition of Banna virus is hitherto unknown in literature and this is the first report of its kind to the best of my knowledge. The functional group and their positions of the benzoxazolone derivative can further be modified to develop a more potent inhibitor against the Banna virus by examining the structure-activity relationships of the newly generated ligands.

4. Methods

4.1. Computational section

4.1.1. Structure based virtual screening

Approximately 27,628 numbers of antiviral molecules from Asinex [21] and Enamine [22] databases were undertaken for the Phase [23] database preparation module. This involved the generation of ionization states at pH 7.0 ± 2.0, removal of high energy ionization/tautomer states and generation of multiple conformers. The prepared Phase databases were then considered for structure based virtual screening process where molecular docking was performed using Glide module [24] of the Schrodinger Small-Molecule Drug Discovery Suite [52]. The structure coordinates of VP9 of Banna virus were collected from the RCSB Protein Data Bank (PDB entry 1W9Z) [15] and processed by the Protein Preparation wizard [25] by adding hydrogen atoms, refining the loop region, and finally energy minimization using an OPLS-2005 force field. The protein, consisting of three similar chains, was divided into three separate protein segments. Each of these segments were analyzed by SiteMap module of the Schrodinger molecular modeling suite [26,27] to identify their binding site and assessing druggability. The prepared Phase database was then subjected to a virtual screening workflow (VSW) consists three steps of docking of increasing precisions, i.e. high-throughput virtual screening (HTVS), standard precision (SP) and extra-precision (XP) [28–30]. At first, all the molecules were screened using HTVS mode and the top 10% of the HTVS output was selected and screened using SP docking mode. Then the top 5% molecules from the SP output were considered and undertaken for docking with XP mode. The output of XP docking was filtered for a docking score of ≤ -7.00 [31,32] and druglikeness according to Lipinski's rule of five [33]. This led to the overall selection of twenty nine ligands for the cross-docking studies with many common interfering proteins for the selective and preferential binding with VP9 of Banna virus.

4.1.2. Cross-docking study

The proteins studied for the cross-selectivity against the selective inhibition of Banna virus are VP7 protein of bluetongue virus (1BVP), dengue virus (1K4R), rhesus rotavirus VP4 (1KRI), dengue 2 virus envelope protein (1OAN), dengue 2 virus envelope protein (1OKE), conserved core domain of venezualan equine encephalitis capsid protein (1EP5 and 1EP6), envelope protein of tick-borne encephalitis virus (1URZ), rotavirus strain DS-1 VP8* core (2AEN), rhesus rotavirus VP5 antigen domain dimer (2B4H), rhesus rotavirus VP8* (2P3I), japanese encephalitis virus envelope protein (3P54), transcribing cypovirus (3J17), porcine CRW-8 rotavirus VP8* (3SIS), cell attachment protein VP8* of a human rotavirus (4DRR), full-length japanese encephalitis virus NS5 (4K6M), apo porcine rotavirus TFR-41 VP8* (5CA6), human rotavirus K8 VP8* (5CB7), P[19] rotavirus VP8* (5VKI) and japanese encephalitis virus (5WSN). A set of five ligands were thus selected, either having no binding or having a docking score of > -7.00 with all of these interfering proteins, for further studies.

4.1.3. Analyzing the molecular properties

The physico-chemical properties of the lead five ligands were evaluated by QikProp and FAFDrugs4 (Free ADME-Tox Filtering Tool) [35]. This is an advanced computational program to predict some properties like adsorption, distribution, metabolism, excretion and toxicity to support hit selection before investing efforts on ligand synthesis or ordering. Also the lead ligands will be assessed for potential Pan Assay Interference Compounds (PAINS) and protein-protein interaction inhibitors (iPPI).

4.1.4. Molecular dynamics simulation

GROMACS 4.6.5 [40–42] software was chosen to set up a simulation system containing the chain A of the protein, VP9, in complex with a ligand, as obtained from the results of docking in XP mode. Each of these complexes were solvated in a similar volume of tip4p water box, energy minimized, equilibrated in NVT and NPT ensemble respectively and finally undertaken for 20 ns of production run (timestep 2 fs) in NPT ensemble at 300 K. GROMOS96 43a1 force field was used in each of the cases. The final trajectories were analyzed using our in-house-developed codes and GROMACS facilities. The various conformations at different time points were monitored to follow the binding efficiency of the ligand with the protein. All of the visualizations were performed with VMD software [53].

4.2. Experimental section

4.2.1. Characterization of the ligand

The hit ligand, benzoxazolone derivative, was procured from a local supplier and characterized for its purity by different analytical techniques like ^{1}H NMR, ^{13}C NMR, high resolution mass spectroscopy (ESI-MS) and its HPLC profile. ^{1}H NMR and ^{13}C NMR spectra were recorded in FT-NMR Bruker DPX 400/500 MHz NMR spectrometer. ESI-MS mass spectra were recorded in QTOF Micro YA263 instrument and the HPLC profile was received from KPC Life Sciences. The molecular formula of the ligand is $C_{17}H_{16}N_2O_4$ and the molecular weight of the ligand is 312.11 Da. The chemical name of the hit ligand is N-(2-(2-(2-oxobenzo[*d*]oxazol-3(2H)-yl)ethoxy)phenyl)acetamide.

4.2.2. Synthesis of the model peptide

The sequence of the model peptide, with which the interaction of the hit ligand can be studied, is AVRMGMQYA. The expected molecular weight of the peptide is 1025.48 Da and the expected molar extinction coefficient is 1490 M^{-1} cm^{-1} (https://web.expasy.org/cgi-bin/protparam/protparam).

The solid phase synthesis of the peptide was followed in a stepwise manner. The Fmoc protected amino acid derivatives were coupled with benzotriazol-1-yl-oxytripyrrolidinophosphonium hexa fluorophosphate (PyBOP)/hydroxybenzotriazole (HOBT)/diisopropylethylamine (DIPEA) (used as 5:5:10 times excess of the resin respectively) and Fmoc clevage was carried out by 20% (v/v) piperidine in dimethylformamide (DMF). 95% trifluoroacetic acid (TFA) in water was used to remove the aliphatic side chains of the peptides from the resin, whereas a cocktail of 85% TFA, 5% H2O, 5% phenol, 2.5% anisole and 2.5% triisopropyl silane was used and kept for an hour while removing the side chain functional group protections of the peptide from the resin. TFA was removed by vacuum evaporation. Rink amide MBHA resin was used during the peptide solid phase preparation.

4.2.3. Purification of the peptide using reverse phase high performance liquid chromatography

The crude peptide was highly hydrophobic and very poorly soluble in water. Therefore the sample was dissolved in 100 mM NaOH and methanol in 1:3 M ratio, vortexed and then purified using reverse phase HPLC (Waters) using a Phenomenix C18 column and CH_3OH-H_2O gradients (0–100% acetonitrile in 60 min) containing 0.1% TFA (figure S4). The final product was characterized by mass spectrometry.

4.2.4. Characterization of the purified peptide/complex using mass spectroscopy

One μL of sample was mixed with 1 μL of matrix (α-cyano-4-hydroxy cinnamic acid, HCCA) and loaded on an Anchor Chip MALDI plate (Bruker Daltonics, Germany). Mass spectra was generated in reflector mode in an Autoflex speed MALDI TOF/TOF (ATS-00069; Bruker Daltonics, Germany) mass spectrometer equipped with a pulsed nitrogen laser in the *m/z* range from 700 to 3500 Da using an Ultraflextreme MALDI-TOF/TOF mass spectrometer controlled by FlexAnalysis software (Bruker Daltonics).

4.2.5. UV–visible spectroscopy

The dissociation constant of the complexes were determined by recording the absorbance spectra in Shimadzu UV-2600 UV–Vis spectrophotometer.

Acknowledgements

PM thanks Department of Science and Technology (DST), Government of India, for the financial support provided through Technical Research Centre (TRC) at IACS (Project No. AI/1/62/IACS/2015). PM is grateful to Prof. Santanu Bhattacharya for his constant encouragements which always help me to give my best.

Appendix A. Supplementary material

Supplementary data to this article can be found online at https://doi.org/10.1016/j.bioorg.2019.01.021.

References

[1] H. Liu, M.-H. Li, Y.-G. Zhai, W.-S. Meng, X.-H. Sun, Y.-X. Cao, S.-H. Fu, H.-Y. Wang, L.-H. Xu, Q. Tang, G.-D. Liang, Emerg. Infect. Dis. 16 (2010) 514–517.
[2] H. Attoui, F.M. Jaafar, P. de Micco, X. de Lamballerie, Emerg. Infect. Dis. 11 (2005) 1673–1679.
[3] H. Liu, X.-Y. Gao, S.-H. Fu, M.-H. Li, Y.-G. Zhai, W.-S. Meng, X.-H. Sun, Z. Lv, H.-Y. Wang, X.-X. Shen, Y.-X. Cao, Y. He, G.-D. Liang, Infect. Genet. Evol. 45 (2016) 250–255.
[4] G. Le Flohic, V. Porphyre, P. Barbazan, J.P. Gonzalez, PLoS Negl. Trop. Dis. 7 (2013) e2208.
[5] L.H. Xu, Y.X. Cao, L.F. He, H.Q. Wang, Y. He, S.H. Fu, X.H. Sun, H.Y. Wang, W.B. Liu, L.H. Wang, G.D. Liang, Zhonghua Shi Yan He Lin Chuang Bing Du Xue Za Zhi 20 (2006) 47–51.
[6] F.M. Jaafar, H. Attoui, P. Gallian, I. Isahak, K.T. Wong, S.K. Cheong, V.S. Nadarajah, J.-F. Cantaloube, P. Biagini, P. De Micco, X. De Lamballerie, J. Virol. Meth. 116 (2004) 55–61.
[7] P. Moitra, D. Bhagat, R. Pratap, S. Bhattacharya, Sci. Rep. 6 (2016) 37355.
[8] N. Dey, S.K. Samanta, S. Bhattacharya, ACS Appl. Mater. Interfaces 5 (2013) 8394–8400.
[9] N. Kumari, N. Dey, S. Bhattacharya, Analyst 139 (2014) 2370–2378.
[10] N. Dey, S. Bhattacharya, Chem. Eur. J. 23 (2017) 16547–16554.
[11] H. Attoui, F. Billoir, P. Biagini, P. de Micco, X. de Lamballerie, J. Gen. Virol. 81 (2000) 1507–1515.
[12] T. Nabeshima, P.T. Nga, P. Guillermo, M.del C. Parquet, F. Yu, N.T. Thuy, B.M. Trang, N.T. Hien, V.S. Nam, S. Inoue, F. Hasebe, K. Morita, Emerg. Infect. Dis. 14 (2008) 1276–1279.
[13] F.M. Jaafar, H. Attoui, P.P.C. Mertens, P. de Micco, X. de Lamballerie, J. Gen. Virol. 86 (2005) 1141–1146.
[14] F.M. Jaafar, H. Attoui, P.P.C. Mertens, P. de Micco, X. de Lamballerie, J. Gen. Virol. 86 (2005) 1147–1157.
[15] F.M. Jaafar, H. Attoui, M.W. Bahar, C. Siebold, G. Sutton, P.P.C. Mertens, P. De Micco, D.I. Stuart, J.M. Grimes, X. De Lamballerie, Structure 13 (2005) 17–28.
[16] K. Zhu, H. Tao, J.-L. Song, L. Jin, Y. Zhang, J. Liu, Z. Chen, C.-S. Jiang, C. Luo, H. Zhang, Bioorg. Chem. 81 (2018) 289–298.
[17] B. Bano, Kanwal, K.M. Khan, F. Begum, M.A. Lodhi, U. Salar, R. Khalil, Z. Ul-Haq, S. Perveen, Bioorg. Chem. 81 (2018) 658–671.
[18] S. Mahmood, A. Saeed, S. Bua, A. Nocentini, P. Gratteri, C.T. Supuran, Bioorg. Chem. 77 (2018) 381–386.
[19] L.-M. Yu, Z. Hu, Y. Chen, A. Ravji, S. Lopez, C.B. Plescia, Q. Yu, H. Yang, M. Abdelmalak, S. Saha, K. Agama, E. Kiselev, C. Marchand, Y. Pommier, L.-K. An, Eur. J. Med. Chem. 151 (2018) 777–796.
[20] P. Kumar, S.O. Silakari, Bioorg. Chem. 79 (2018) 163–170.
[21] J.H. Voigt, B. Bienfait, S. Wang, M.C. Nicklaus, J. Chem. Inf. Comput. Sci. 41 (2001) 702–712.
[22] A. Del Rio, A.J.M. Barbosa, F. Caporuscio, G.F. Mangiatordi, Mol. BioSyst. 6 (2010) 2122–2128.
[23] S.L. Dixon, A.M. Smondyrev, E.H. Knoll, S.N. Rao, D.E. Shaw, R.A. Friesner, J. Comput.-Aided Mol. Des. 20 (2006) 647–671.
[24] R.A. Friesner, J.L. Banks, R.B. Murphy, T.A. Halgren, J.J. Klicic, D.T. Mainz, M.P. Repasky, E.H. Knoll, M. Shelley, J.K. Perry, J. Med. Chem. 47 (2004) 1739–1749.
[25] G.M. Sastry, M. Adzhigirey, T. Day, R. Annabhimoju, W. Sherman, J. Comput. Aid. Mol. Des. 27 (2013) 221–234.
[26] T. Halgren, J. Chem. Inf. Model. 49 (2009) 377–389.
[27] T. Halgren, Chem. Biol. Drug Des. 69 (2007) 146–148.
[28] T. Tamilvanan, W. Hopper, Bioinformation 9 (2013) 286–292.
[29] T.A. Halgren, R.B. Murphy, R.A. Friesner, H.S. Beard, L.L. Frye, W.T. Pollard, J.L. Banks, J. Med. Chem. 47 (2004) 1750–1759.
[30] R.A. Friesner, R.B. Murphy, M.P. Repasky, L.L. Frye, J.R. Greenwood, T.A. Halgren, P.C. Sanschagrin, D.T. Mainz, J. Med. Chem. 49 (2006) 6177–6196.
[31] L. Zaccagnini, S. Brogi, M. Brindisi, S. Gemma, G. Chemi, G. Legname, G. Campiani, S. Butini, Eur. J. Med. Chem. 127 (2017) 859–873.
[32] J. Guo, S. Durdagi, M. Changalov, L. Perissinotti, J.M. Hargreaves, T.G. Back, S.Y. Noskov, H.J. Duff, PLoS One 9 (2014) e105553.
[33] C.A. Lipinski, J. Pharmacol. Toxicol. Meth. 44 (2000) 235–249.
[34] M. Rashid, A. Husain, M. Shaharyar, R. Mishra, A. Hussain, O. Afzal, Eur. J. Med. Chem. 83 (2014) 630–645.
[35] D. Lagorce, L. Bouslama, J. Becot, M.A. Miteva, B.O. Villoutreix, Bioinformatics 33 (2017) 3658–3660.
[36] J.B. Baell, G.A. Holloway, J. Med. Chem. 53 (2010) 2719–2740.
[37] O. Sperandio, C.H. Reynes, A.C. Camproux, B.O. Villoutreix, Drug Discov. Today 15 (2010) 220–229.
[38] C. Reynes, H. Host, A.C. Camproux, G. Laconde, F. Leroux, A. Mazars, B. Deprez, R. Fahraeus, B.O. Villoutreix, O. Sperandio, PLoS Comput. Biol. 6 (2010) e1000695.
[39] T.W. Johnson, K.R. Dress, M. Edwards, Bioorg. Med. Chem. Lett. 19 (2009) 5560–5564.
[40] S. Pronk, S. Pall, R. Schulz, P. Larsson, P. Bjelkmar, R. Apostolov, M.R. Shirts, J.C. Smith, P.M. Kasson, D. van der Spoel, B. Hess, E. Lindahl, Bioinformatics 29 (2013) 845–854.
[41] B. Hess, C. Kutzner, D. van der Spoel, E. Lindahl, J. Chem. Theory Comput. 4 (2008) 435–447.
[42] D. van der Spoel, E. Lindahl, B. Hess, G. Groenhof, A.E. Mark, H.J.C. Berendsen, J. Comput. Chem. 26 (2005) 1701–1718.
[43] P. Moitra, Y. Subramanian, S. Bhattacharya, J. Phys. Chem. B 121 (2017) 815–824.
[44] A. Ali, M. Bansal, S. Bhattacharya, J. Phys. Chem. B 119 (2015) 5–14.
[45] J. Poupaert, P. Carato, E. Colacino, Curr. Med. Chem. 12 (2005) 877–885.
[46] Z. Soyer, B. Erac, FABAD J. Pharm. Sci. 32 (2007) 167–171.
[47] Y. Mulazim, C. Berber, H. Erdogan, M.H. Ozkan, B. Kesanli, EuroBiotech 1 (2017) 1–6.
[48] D. Pizzirani, A. Bach, N. Realini, A. Armirotti, L. Mengatto, I. Bauer, S. Girotto, C. Pagliuca, M.D. Vivo, M. Summa, A. Ribeiro, D. Piomelli, Angew. Chem. Int. Ed. 54 (2015) 485–489.
[49] M. Koksal, N.G. Kelekci, G.O. Mercanoglu, H. Erdogan, Arzneimittel-Forschung (Drug Res.) 58 (2008) 398–404.
[50] M. Vijayasarathy, P. Balaram, Toxicon 144 (2018) 68–74.
[51] D. Suckau, A. Resemann, M. Schuerenberg, P. Hufnagel, J. Franzen, A. Holle, Anal. Bioanal. Chem. 376 (2003) 952–965.
[52] Y. Jia, T.L. Chiu, E.A. Amin, V. Polunovsky, P.B. Bitterman, C.R. Wagner, Eur. J. Med. Chem. 45 (2010) 1304–1313.
[53] W. Humphrey, A. Dalke, K. Schulten, J. Mol. Graph. 14 (1996) 33–38.